April, 2009

Analytical solution for Stokes flow inside an evaporating sessile drop: Spherical and cylindrical cap shapes

Hassan Masoud, *State University of New York at Buffalo*
James D. Felske, *State University of New York at Buffalo*

Analytical solution for Stokes flow inside an evaporating sessile drop: Spherical and cylindrical cap shapes

Hassan Masoud, and James D. Felske

Citation: Physics of Fluids **21**, 042102 (2009); doi: 10.1063/1.3112002
View online: http://dx.doi.org/10.1063/1.3112002
View Table of Contents: http://aip.scitation.org/toc/phf/21/4
Published by the American Institute of Physics

Analytical solution for Stokes flow inside an evaporating sessile drop: Spherical and cylindrical cap shapes

Hassan Masoud[a] and James D. Felske
Department of Mechanical and Aerospace Engineering, State University of New York at Buffalo, Buffalo, New York 14260, USA

(Received 18 December 2008; accepted 10 March 2009; published online 10 April 2009)

Exact analytical solutions are derived for the Stokes flows within evaporating sessile drops of spherical and cylindrical cap shapes. The results are valid for all contact angles. Solutions are obtained for arbitrary evaporative flux distributions along the free surface as long as the flux is bounded at the contact line. Specific results and computations are presented for evaporation corresponding to uniform flux and to purely diffusive gas phase transport into an infinite ambient. Wetting and nonwetting contact angles are considered with the flow patterns in each case being illustrated. For the spherical cap with evaporation controlled by vapor phase diffusion, when the contact angle lies in the range $0 \leq \theta_c < \pi/2$, the mass flux of vapor becomes singular at the contact line. This condition requires modification when solving for the liquid-phase transport. Droplets in all of the above categories are considered for the following two cases: the contact lines are either pinned or free to move during evaporation. The present viscous flow behavior is compared to the inviscid flow behavior previously reported. It is seen that the streamlines for viscous flow lie farther from the substrate than the corresponding inviscid ones. © *2009 American Institute of Physics*.
[DOI: 10.1063/1.3112002]

I. INTRODUCTION

When a sessile droplet containing solid constituents dries on a substrate, the solute particles deposit on the surface in various patterns. The final deposition pattern and the ability to control it are of high interest for many industrial and scientific processes. Examples are the creation of an ordered array of semiconductor nanoparticles for electronics[1] or DNA molecules for gene expression analysis.[2] Also, evaporation-driven flow is used to assemble two-dimensional (2D) crystals in protein crystallography.[3–5] Moreover, a particular deposition pattern—the ring shape—has important implications for DNA stretching,[6] ink-jet printing,[7–9] and coatings.

The deposition pattern produced depends on the flow within the drop. As shown previously,[10] the flow pattern strongly depends on the combination of evaporative flux, shape of the free surface, and behavior of the contact line. For instance, flow can be toward, away, or both toward and away from the contact line under different combinations of these factors.

Flow inside an evaporating sessile droplet has been studied analytically, semianalytically, and numerically. Deegan *et al.*[11–13] and Popov[14] utilized the vertically averaged velocity in considering the behavior of velocities at small contact angles. Solutions in the limit of lubrication theory were obtained numerically by Fischer[15] and semianalytically by Hu and Larson.[16] Stokes flow for contact angles ranging from 0° to 90° was evaluated numerically by Hu and Larson[16] and Widjaja *et al.*[17] The exact analytical solution for irrotational flow was derived for hemispheres by Tarasevich,[18] for spherical caps by Masoud and Felske,[10] and for hemicylinders and cylindrical caps by Petsi and Burganos.[19,20]

The present study considers the exact analytical solutions for Stokes flows within evaporating, sessile, spherical and cylindrical cap drops. The full range of contact angles ($0 < \theta_c < \pi$) are considered as well as arbitrary distributions of evaporative flux along the free surface. The contact line of the droplet is allowed to be either pinned or free to move during evaporation. Analytical expressions for the expansion coefficients are given for the case of uniform flux. To the best of our knowledge, the Stokes flow within an evaporating, sessile, nonwetting drop has not been reported by any approach, analytical or numerical.

II. MODEL DEVELOPMENT AND SOLUTIONS

The droplets considered in the present study are ~1 mm from the axis of symmetry to the contact line (R). For water drops of this size evaporating under room conditions, the characteristic velocity in the drop is ~1 μm/s with a corresponding Reynolds number of $\sim 10^{-3}$.[16] For such flows, inertial forces are negligible (Stokes flow) and the continuity, momentum, and vorticity equations become

$$\nabla \cdot \mathbf{V} = 0, \tag{1}$$

$$\mu \nabla^2 \mathbf{V} = \nabla p, \tag{2}$$

and

$$\nabla^2 \boldsymbol{\omega} = 0, \tag{3}$$

where $\mathbf{V}$ is the fluid velocity, p is the difference between the thermodynamic (P) and hydrostatic (p_h) pressures ($p = P$

[a]Author to whom correspondence should be addressed. Electronic mail: hmasoud@eng.buffalo.edu.

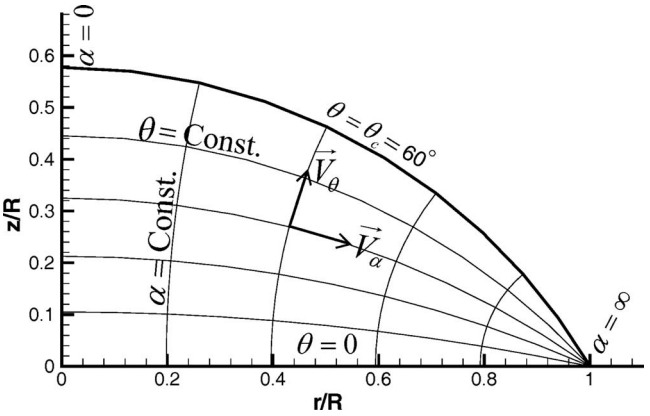

FIG. 1. Toroidal coordinates: lines of constant α and θ; positive velocity components.

$-p_h$), and $\boldsymbol{\omega}=\nabla\times\mathbf{V}$ is the vorticity. The application of these equations to the two geometries of interest will now be considered.

A. Spherical cap shape

1. Geometry

The shape acquired by a drop on a substrate is determined by surface tension, gravity, and the fluid flows within and over the surface of the droplet. For a stagnant external fluid, the relative importance of the remaining quantities may be assessed from the Bond and capillary numbers. The Bond number is the ratio of gravitational to surface tension forces: $\mathrm{Bo}=\rho g R_c h_{\max}/\sigma$, where R_c, $h_{\max}$, and σ are, respectively, the droplet's mean radius of curvature, the droplet's maximum height, and the surface tension. The capillary number is the ratio of viscous to surface tension forces; $\mathrm{Ca}=\mu V_0/\sigma$, where μ is the viscosity and V_0 is a characteristic velocity. For millimeter size water drops, $\mathrm{Bo}=\sim 0.04$ and $\mathrm{Ca}=\sim 10^{-8}$. Hence, surface tension is the dominant influence on the droplet's shape, and the droplet becomes a spherical cap. It is also noted from Eq. (2) that the pressure gradient (∇p) and the viscous forces ($\mu\nabla^2 V$) are equal. Then, since $\mathrm{Ca}/\mathrm{Bo}\sim 10^{-7}$ $\sim$(viscous/gravitational)$\sim$(∇p/gravitational), the thermodynamic pressure (P) variation throughout the drop is essentially equal to the hydrostatic pressure variation (p_h).

The hemispherical cap geometry is a sphere cut by a plane. Since this shape and the boundary conditions being considered are azimuthally independent, so is the flow within the drop. The natural coordinates are therefore toroidal. Figure 1 shows a cross section of this geometry at a given azimuthal angle φ. The metric coefficients for the toroidal coordinates are

$$h_\alpha = h_\theta = h_\phi/\sinh\alpha = R(\cosh\alpha+\cos\theta)^{-1}, \tag{4}$$

where, $0\le\alpha\le\infty$, $-\pi\le\theta\le\pi$, and $0\le\varphi\le 2\pi$. In presenting results it is often clearer to use cylindrical coordinates (r,θ). The relationships between the two systems are

$$r/\sinh\alpha = z/\sin\theta = R(\cosh\alpha+\cos\theta)^{-1}. \tag{5}$$

2. Field equation

For 2D and three-dimensional (3D) axisymmetric flows, velocity components may be expressed in terms of a stream function. The stream function ψ is defined to satisfy the continuity equation,

$$V_\alpha = \frac{1}{h_\theta h_\varphi}\frac{\partial\psi}{\partial\theta} = \frac{(\cosh\alpha+\cos\theta)^2}{R^2\sinh\alpha}\frac{\partial\psi}{\partial\theta}, \tag{6}$$

$$V_\theta = -\frac{1}{h_\varphi h_\alpha}\frac{\partial\psi}{\partial\alpha} = -\frac{(\cosh\alpha+\cos\theta)^2}{R^2\sinh\alpha}\frac{\partial\psi}{\partial\alpha}. \tag{7}$$

The field equation for ψ follows from writing Eq. (3) for axially symmetric flow. Substituting from above for V_α and V_θ in terms of ψ shows that the vorticity is related to the stream function by

$$\boldsymbol{\omega} = (\hat{\mathbf{e}}_\varphi/h_\varphi)E^2\psi, \tag{8}$$

where

$$E^2\psi = \frac{\sinh\alpha(\cosh\alpha+\cos\theta)}{R^2}\left[\frac{\partial}{\partial\alpha}\left(\frac{\cosh\alpha+\cos\theta}{\sinh\alpha}\frac{\partial\psi}{\partial\alpha}\right) + \frac{\partial}{\partial\theta}\left(\frac{\cosh\alpha+\cos\theta}{\sinh\alpha}\frac{\partial\psi}{\partial\theta}\right)\right]. \tag{9}$$

Repeated application of the curl operator to Eq. (8) results in

$$\nabla^2\boldsymbol{\omega} = \nabla\times(\nabla\times\boldsymbol{\omega}) = -(\hat{\mathbf{e}}_\varphi/h_\varphi)E^2(E^2\psi). \tag{10}$$

Consequently, the field equation for ψ, which corresponds to $\nabla^2\boldsymbol{\omega}=0$, is

$$E^4\psi = 0. \tag{11}$$

3. Integration of $E^4\psi=0$

The analytical solution to $E^4\psi=0$ subject to appropriate boundary conditions is considered in this section. In toroidal coordinates the integration of $E^4\psi=0$ has been accomplished using different analytical techniques.[21–23] Stimson and Jefferey[21] first integrated $E^2(\psi)$ and then transformed this result into cylindrical coordinates. They completed the integration of $E^4(\psi)=0$ by exploiting the (coordinate) linearity of the cylindrical operator in the axial direction. Khuri and Wazwaz[23] employed the method of separation of variables and achieved a solution in terms of eigenfunctions in the θ-coordinate. The present study requires eigenfunctions in the α-coordinate in order to represent arbitrary variations in the evaporative flux distribution. In Appendix A, using separation of variables, it is shown that the required eigenfunctions are Gegenbauer functions and that the general form of the solution is

$$\psi(\alpha,\theta) = (\cosh\alpha+\cos\theta)^{-3/2}\int_0^\infty [A(\tau)C^{-1/2}_{1/2+i\tau}(\cosh\alpha) + B(\tau)C^{*-1/2}_{1/2+i\tau}(\cosh\alpha)] \times\{\sinh(\tau\theta)[C(\tau)\sin\theta+D(\tau)\cos\theta] + \cosh(\tau\theta)[E(\tau)\sin\theta+F(\tau)\cos\theta]\}d\tau \tag{12}$$

where $C_{1/2+i\tau}^{-1/2}$ and $C_{1/2+i\tau}^{*-1/2}$ are Gegenbauer functions of the first and second kinds, of order of $-1/2$. (Note that Payne and Pell[22] used a different approach for obtaining the general solution.)

To establish boundary conditions on the stream function ψ, it is first noted that the velocity components normal to the axis of symmetry and normal to the solid surface vanish: $V_\alpha(0,\theta)=0$ and $V_\theta(\alpha,0)=0$. Hence, the stream function is constant along the axis of symmetry and along the solid surface. Since these surfaces intersect, the constant must be the same for both surfaces. It is arbitrarily set to zero since its value does not affect the predicted velocities. The no slip condition requires that the velocity component tangent to the solid surface vanishes at the surface, $V_\alpha(\alpha,0)=0$. Along the axis of symmetry, derivatives normal to the axis are zero; in particular, $\partial V_\theta/\partial\alpha|_{\alpha=0}=0$. The corresponding boundary conditions on ψ are

$$\psi(0,\theta)=0, \tag{13}$$

$$\psi(\alpha,0)=0, \tag{14}$$

$$\left.\frac{\partial\psi}{\partial\theta}\right|_{\theta=0}=0, \tag{15}$$

and

$$\frac{\partial}{\partial\alpha}\left[\frac{(\cosh\alpha+\cos\theta)^2}{\sinh\alpha}\frac{\partial\psi}{\partial\alpha}\right]_{\alpha=0}=0. \tag{16}$$

Applying these conditions to Eq. (12), it follows from Eq. (13) that $B(\tau)=0$;[10] from Eq. (14),

$$F(\tau)=0, \tag{17}$$

and, from Eq. (15),

$$E(\tau)+\tau D(\tau)=0. \tag{18}$$

Incorporating these into Eq. (12), the stream function becomes

$$\psi(\alpha,\theta)=(\cosh\alpha+\cos\theta)^{-3/2}\times\int_0^\infty K(\theta,\tau)C_{1/2+i\tau}^{-1/2}(\cosh\alpha)d\tau, \tag{19}$$

where

$$K(\theta,\tau)=k_1(\tau)\sin\theta\sinh(\tau\theta)+k_2(\tau)[\cos\theta\sinh(\tau\theta)-\tau\sin\theta\cosh(\tau\theta)]. \tag{20}$$

In the third and fourth boundary conditions in the α-direction, in order for the integrals to exist the velocity components must be nonsingular (finite) at the contact line

$$\lim_{\alpha\to\infty}\left[\frac{(\cosh\alpha+\cos\theta)^2}{\sinh\alpha}\frac{\partial\psi}{\partial\theta}\right]=\text{finite} \tag{21}$$

and

$$\lim_{\alpha\to\infty}\left[\frac{(\cosh\alpha+\cos\theta)^2}{\sinh\alpha}\frac{\partial\psi}{\partial\alpha}\right]=\text{finite}. \tag{22}$$

These two conditions and Eq. (16) are satisfied for physically meaningful distributions of evaporative flux at the free surface.

The unknown coefficients, $k_1(\tau)$ and $k_2(\tau)$, can be obtained from the distribution of the stream function at the free surface in conjunction with the zero shear stress boundary condition, $\tau_{\alpha\theta}(\alpha,\theta_c)=0$. $K(\theta_c,\tau)$ can be written in terms of the stream function at the free surface using the integral transform presented in Ref. 10,

$$K(\theta_c,\tau)=\tau(\tau^2+1/4)\tanh(\pi\tau)\times\int_0^\infty\frac{\psi(\alpha,\theta_c)(\cosh\alpha+\cos\theta_c)^{3/2}}{\sinh\alpha}\times C_{1/2+i\tau}^{-1/2}(\cosh\alpha)d\alpha. \tag{23}$$

Using Eqs. (4–14.1), (4–14.2), and (A-7.7) of Ref. 24, vanishing of the shear stress at the free surface gives

$$\tau_{\alpha\theta}|_{\theta=\theta_c}=-\mu\left\{\frac{\partial}{\partial\alpha}[(\cosh\alpha+\cos\theta)(V_\theta/R)]+\frac{\partial}{\partial\theta}[(\cosh\alpha+\cos\theta)(V_\alpha/R)]\right\}_{\theta=\theta_c}=0. \tag{24}$$

Therefore,

$$\tilde{K}(\theta_c,\tau)=\tau(\tau^2+1/4)\tanh(\pi\tau)\times\int_0^\infty\frac{\tilde{\psi}(\alpha,\theta_c)}{\sinh\alpha}C_{1/2+i\tau}^{-1/2}(\cosh\alpha)d\alpha, \tag{25}$$

in which

$$\tilde{\psi}(\alpha,\theta_c)=-(\cosh\alpha+\cos\theta_c)^{-1/2}\times\left\{\frac{R^2\sinh\alpha}{\cosh\alpha+\cos\theta_c}\frac{\partial}{\partial\alpha}\times[(\cosh\alpha+\cos\theta_c)V_\theta(\alpha,\theta_c)]+\frac{3\psi(\alpha,\theta_c)}{2}\times[\cos\theta_c(\cosh\alpha+\cos\theta_c)-\sin^2\theta_c/2]\right\} \tag{26}$$

and

$$\tilde{K}(\theta_c,\tau)=\frac{\partial^2}{\partial^2\theta}K(\theta_c,\tau)=k_1(\tau)[(\tau^2-1)\sin\theta_c\sinh(\tau\theta_c)+2\tau\cos\theta_c\cosh(\tau\theta_c)]-k_2(\tau)(\tau^2+1)\times[\cos\theta_c\sinh(\tau\theta_c)+\tau\sin\theta_c\cosh(\tau\theta_c)]. \tag{27}$$

Using Eqs. (23) and (25), the coefficients $k_1(\tau)$ and $k_1(\tau)$ are found to be

$$k_1(\tau) = \frac{N_2(\tau,\theta_c)K(\tau,\theta_c) + N_1(\tau;\theta_c)\tilde{K}(\tau,\theta_c)}{N_2(\tau,\theta_c)M_1(\tau,\theta_c) + N_1(\tau,\theta_c)M_2(\tau,\theta_c)} \tag{28}$$

and

$$k_2(\tau) = \frac{M_2(\tau,\theta_c)K(\tau,\theta_c) - M_1(\tau,\theta_c)\tilde{K}(\tau,\theta_c)}{N_2(\tau,\theta_c)M_1(\tau,\theta_c) + N_1(\tau,\theta_c)M_2(\tau,\theta_c)}, \tag{29}$$

where

$$M_1(\tau,\theta_c) = \sin\ \theta_c\ \sinh(\tau\theta_c), \tag{30}$$

$$M_2(\tau,\theta_c) = (\tau^2 - 1)\sin\ \theta_c\ \sinh(\tau\theta_c) + 2\tau\cos\ \theta_c\ \cosh(\tau\theta_c), \tag{31}$$

$$N_1(\tau,\theta_c) = \cos\ \theta\ \sinh(\tau\theta) - \tau\sin\ \theta\ \cosh(\tau\theta), \tag{32}$$

and

$$N_2(\tau,\theta_c) = (\tau^2 + 1)[\cos\ \theta_c\ \sinh(\tau\theta_c) + \tau\sin\ \theta_c\ \cosh(\tau\ \theta_c)]. \tag{33}$$

The final boundary condition is the known distribution of evaporative flux along the free surface. This distribution is determined by the gas phase mass transport and is independent of the flow within the drop. The velocity and stream function at the free surface follow directly from this flux. The velocity is obtained from mass conservation, whereby the mass flux in the liquid equals the mass flux in the gas. In terms of the liquid, the evaporation rate is

$$J(\alpha) = \rho[V_\theta(\alpha,\theta_c) - V_{\theta,B}(\alpha)], \tag{34}$$

where $J(\alpha)$ is the evaporative flux at the free surface, ρ is the liquid density, and $V_{\theta,B}$ is the speed at which the boundary is moving in the direction normal to itself. From Eq. (7), the boundary condition on ψ may then be written in terms of $V_\theta(\alpha,\theta_c)$,

$$\psi(\alpha,\theta_c) = -\int_0^\alpha \frac{R^2\sinh\alpha'}{(\cosh\alpha' + \cos\theta_c)^2} V_\theta(\alpha',\theta_c)d\alpha' = -\int_0^\alpha \frac{R^2\sinh\alpha'}{(\cosh\alpha' + \cos\theta_c)^2}[J(\alpha')/\rho + V_{\theta,B}(\alpha')]d\alpha'. \tag{35}$$

Finally, from $\psi(\alpha,\theta)$, the velocity distribution may be calculated. The velocity components in toroidal coordinates follow from Eqs. (6) and (7),

$$V_\alpha(\alpha,\theta) = \frac{\sqrt{\cosh\alpha + \cos\theta}}{R^2\sinh\alpha}\times\left[(3\sin\theta/2)\sqrt{\cosh\alpha + \cos\theta}\psi(\alpha,\theta) + \int_0^\infty \frac{\partial K(\theta,\tau)}{\partial\theta} C_{1/2+i\tau}^{-1/2}(\cosh\alpha)d\tau\right], \tag{36}$$

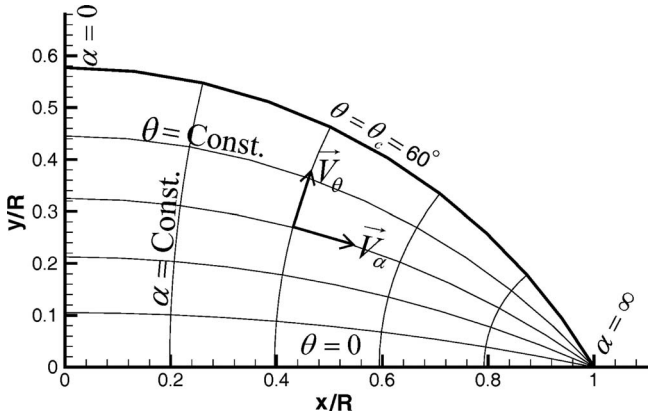

FIG. 2. Bipolar coordinates: lines of constant α and θ; positive velocity components.

$$V_\theta(\alpha,\theta) = \frac{\sqrt{\cosh\alpha + \cos\theta}}{R^2}\left\{\frac{3\sqrt{\cosh\alpha + \cos\theta}\psi(\alpha,\theta)}{2} + \int_0^\infty K(\theta,\tau)P_{-1/2+i\tau}(\cosh\alpha)d\tau\right\}, \tag{37}$$

where $P_{-1/2+i\tau}(x)$ is the conical function of the first kind. For visualizing and interpreting the flow field, the velocity components in cylindrical coordinates are useful. The radial and axial components of the velocity are given by

$$V_r(\alpha,\theta) = r^{-1}(\partial\psi/\partial z) = (\cosh\alpha + \cos\theta)^{-1}[V_\alpha(1 + \cosh\alpha\cos\theta) + V_\theta\sinh\alpha\sin\theta], \tag{38}$$

$$V_z(\alpha,\theta) = -r^{-1}(\partial\psi/\partial x) = -(\cosh\alpha + \cos\theta)^{-1}[V_\alpha\sinh\alpha\sin\theta - V_\theta\times(1 + \cosh\alpha\cos\theta)]. \tag{39}$$

B. Cylindrical cap shape

1. Geometry

Similar to spherical drops, the sizes of the 2D liquid lines being considered are small enough that surface tension is the dominant force defining their cross-sectional shape. Consequently, they have the cylindrical cap geometry whose free surface is exactly mapped in bipolar coordinates. Bipolar coordinates (α,θ) are shown in Fig. 2 along with Cartesian coordinates (x,y). (Note that the cross section of a cylindrical cap in bipolar coordinates is identical to the cross section of a spherical cap in toroidal coordinates, Fig. 1.) The metric coefficients for bipolar geometry are

$$h_\alpha = h_\theta = R(\cosh\alpha + \cos\theta)^{-1}, \tag{40}$$

where $-\infty \le \alpha \le \infty$ and $-\pi \le \theta \le \pi$. Bipolar and Cartesian coordinates are related by

$$x/\sinh\alpha = y/\sin\theta = R(\cosh\alpha + \cos\theta)^{-1}. \tag{41}$$

2. Field equation

Based on the definition of the stream function ψ, the velocity components are given by

$$V_\alpha = \frac{1}{h_\theta}\frac{\partial \psi}{\partial \theta} = \frac{\cosh\alpha + \cos\theta}{R}\frac{\partial \psi}{\partial \theta}, \tag{42}$$

$$V_\theta = -\frac{1}{h_\alpha}\frac{\partial \psi}{\partial \alpha} = -\frac{\cosh\alpha + \cos\theta}{R}\frac{\partial \psi}{\partial \alpha}. \tag{43}$$

The field equation for ψ follows from Eq. (2) by substituting the above for V_α and V_θ. For 2D flows, the vorticity is related to the stream function by

$$\boldsymbol{\omega} = \hat{\mathbf{e}}_z \nabla^2 \psi, \tag{44}$$

where

$$\nabla^2 \psi = \frac{(\cosh\alpha + \cos\theta)^2}{R^2}\left(\frac{\partial^2 \psi}{\partial \alpha^2} + \frac{\partial^2 \psi}{\partial \theta^2}\right). \tag{45}$$

Hence, the field equation for ψ, corresponding to $\nabla^2\boldsymbol{\omega}=0$, is

$$\nabla^4 \psi = 0. \tag{46}$$

3. Integration of $\nabla^4\psi=0$

Jeffery[25] integrated of $\nabla^4\psi=0$ in bipolar coordinates obtaining a solution in terms of eigenfunctions in the θ-coordinate. In the present study, eigenfunctions are required in the α-coordinate. In Appendix B, using separation of variables, it is shown that the appropriate solution is

$$\psi(\alpha,\theta) = (\cosh\alpha + \cos\theta)^{-1}\int_0^\infty [A(\tau)\sin(\tau\alpha) + B(\tau)\cos(\tau\alpha)] \times \{\sinh(\tau\theta)[C(\tau)\sin\theta + D(\tau)\cos\theta] + \cosh(\tau\theta)[E(\tau)\sin\theta + F(\tau)\cos\theta]\}d\tau. \tag{47}$$

The forms of the solutions for the 2D and 3D axisymmetric cases are similar and the boundary conditions are the same. Consequently, the forms of the results for spherical caps [Eqs. (23)–(33)] apply to cylindrical caps as well. Using Eqs. (23)–(33), the bipolar stream function, Eq. (47), becomes

$$\psi(\alpha,\theta) = (\cosh\alpha + \cos\theta)^{-1}\int_0^\infty K(\theta,\tau)\sin(\tau\alpha)d\tau. \tag{48}$$

Taking into account that $\sin(\tau\alpha)$ is the eigenfunction of Eq. (48),

$$K(\tau,\theta_c) = \frac{2}{\pi}\int_0^\infty \psi(\alpha,\theta_c)(\cosh\alpha + \cos\theta_c)\sin(\tau\alpha)d\alpha. \tag{49}$$

Equation (24) is also valid in bipolar coordinates but the definitions of V_α and V_θ in terms of the stream function are different. Consequently, the zero shear stress boundary condition yields

$$\tilde{K}(\tau,\theta_c) = \frac{2}{\pi}\int_0^\infty \tilde{\tilde{\psi}}(\alpha,\theta_c)\sin(\tau\alpha)d\alpha, \tag{50}$$

in which

$$\tilde{\tilde{\psi}}(\alpha,\theta_c) = -\frac{R}{\cosh\alpha + \cos\theta_c}\frac{\partial}{\partial\alpha}[(\cosh\alpha + \cos\theta_c)V_\theta(\alpha,\theta_c)] + \cos\theta_c\psi(\alpha,\theta_c). \tag{51}$$

Knowing $K(\tau,\theta_c)$ and $\tilde{K}(\tau,\theta_c)$, the unknown coefficients, $k_1(\tau)$ and $k_2(\tau)$, are then obtained from Eqs. (28) and (29).

Similar to the spherical cap case, the evaporation rate is related to the variation along the interface of the velocity component normal to the interface, Eq. (34). Using Eqs. (34) and (43), the distribution of the stream function along the surface of the droplet may be written in terms of $V_\theta(\alpha,\theta_c)$,

$$\psi(\alpha,\theta_c) = -\int_0^\alpha \frac{R\sinh\alpha'}{\cosh\alpha' + \cos\theta_c}V_\theta(\alpha',\theta_c)d\alpha' = -\int_0^\alpha \frac{R\sinh\alpha'}{\cosh\alpha' + \cos\theta_c}[J(\alpha')/\rho + V_{\theta,B}(\alpha')]d\alpha'. \tag{52}$$

In bipolar coordinates, the components of the velocity follow from Eqs. (42) and (43),

$$RV_\alpha(\alpha,\theta) = \sin\theta\psi(\alpha,\theta) + \int_0^\infty \frac{\partial K(\theta,\tau)}{\partial\theta}\sin(\tau\alpha)d\tau, \tag{53}$$

$$RV_\theta(\alpha,\theta) = \sinh\alpha\psi(\alpha,\theta) + \int_0^\infty K(\theta,\tau)\cos(\tau\alpha)\tau d\tau. \tag{54}$$

In Cartesian coordinates the horizontal and vertical components of the velocity are

$$V_x(\alpha,\theta) = \partial\psi/\partial y = (\cosh\alpha + \cos\theta)^{-1}[V_\alpha(1 + \cosh\alpha\cos\theta) + V_\theta\sinh\alpha\sin\theta], \tag{55}$$

$$V_y(\alpha,\theta) = -\partial\psi/\partial x = -(\cosh\alpha + \cos\theta)^{-1}[V_\alpha\sinh\alpha\sin\theta - V_\theta \times (1 + \cosh\alpha\cos\theta)]. \tag{56}$$

III. PINNED CONTACT LINE

When the droplet is "pinned" at the contact line, R is constant and $\theta_c = \theta_c(t)$. This condition will be considered for spherical caps first followed by cylindrical caps. For each of these geometries, two different evaporative fluxes will be considered: uniform and gas-diffusion controlled.

A. Spherical cap shape

As reported previously,[10]

$$\frac{d\theta_c}{dt} = -(2/R)(1+\cos\theta_c)^2 \times \int_0^\infty \frac{\sinh\alpha}{(\cosh\alpha+\cos\theta_c)^2}\frac{J(\alpha)}{\rho}d\alpha, \tag{57}$$

$$V_\theta(\alpha,\theta_c) = R(\cosh\alpha+\cos\theta_c)^{-1}(d\theta_c/dt) + J(\alpha)/\rho, \tag{58}$$

and

$$\psi(\alpha,\theta_c) = -\frac{d\theta_c}{dt}\frac{R^3}{2}\left[\frac{1}{(1+\cos\theta_c)^2} - \frac{1}{(\cosh\alpha+\cos\theta_c)^2}\right] - \int_0^\alpha \frac{R^2\sinh\alpha'}{(\cosh\alpha'+\cos\theta_c)^2}\frac{J(\alpha')}{\rho}d\alpha'. \tag{59}$$

Any physically obtainable distribution of evaporative flux may be considered. Many are possible since different distributions result from different combinations of gas phase velocities and degrees of vacuum into which the evaporation occurs. Two specific cases are considered below.

1. Uniform evaporative flux

In this case, the evaporative flux is uniform across the surface of the drop,

$$J(\alpha,\theta_c) = \text{const} = J_0. \tag{60}$$

Therefore,

$$\frac{d\theta_c}{dt} = -\frac{2J_0}{R\rho}(1+\cos\theta_c), \tag{61}$$

$$V_\theta(\alpha,\theta_c) = (J_0/\rho)[1-2(1+\cos\theta_c)/(\cosh\alpha+\cos\theta_c)], \tag{62}$$

and

$$\psi(\alpha,\theta_c) = \frac{R^2J_0}{\rho(\cosh\alpha+\cos\theta_c)}\left(1-\frac{1+\cos\theta_c}{\cosh\alpha+\cos\theta_c}\right). \tag{63}$$

Consequently,

$$\tilde{\psi}(\theta_c,\tau) = (R^2J_0/\rho)\left[-\sqrt{\cosh\alpha+\cos\theta_c} + \frac{\cos\theta_c/2}{\sqrt{\cosh\alpha+\cos\theta_c}} + \frac{4-(\cos\theta_c-3)^2/4}{(\cosh\alpha+\cos\theta_c)^{3/2}} - \frac{3\sin^2\theta_c(1+\cos\theta_c)/4}{(\cosh\alpha+\cos\theta_c)^{5/2}}\right]. \tag{64}$$

Using Eqs. (23) and (25) in conjunction with Eq. (A15) of Ref. 10,

$$K(\theta_c,\tau) = -(R^2J_0/\rho)(\sqrt{2}\cosh\pi\tau)^{-1}[2\tau\cot(\theta_c/2)\sinh\theta_c\tau + \cosh\theta_c\tau] \tag{65}$$

and

$$\tilde{K}(\theta_c,\tau) = \frac{R^2J_0}{\rho\sqrt{8}\cosh\pi\tau\sin^2(\theta_c/2)}\{2\tau\sinh\theta_c\tau\cot(\theta_c/2) \times[\tau^2(\cos\theta_c-1)-2\cos\theta_c-1] + \cosh\theta_c\tau[\tau^2(5\cos\theta_c+7)-\cos\theta_c+1]\}. \tag{66}$$

2. Diffusive evaporative flux

A commonly considered flux distribution corresponds to diffusive mass transfer into a stagnant gas (i.e., absent even the gas motion which occurs naturally due to the mass transfer). This model leads to Laplace's equation in toroidal coordinates for the variation in vapor concentration throughout the gas phase. Solving this equation results in the nonphysical (singular) evaporative flux at the contact line ($\alpha\to\infty$) for cases of wetting contact angles: $0\le\theta_c<\pi/2$.[14] From previous work,[10] it is known that the Gegenbauer transforms exist provided that $\lim_{\alpha\to\infty}[\psi(\alpha,\theta_c)(\cosh\alpha+\cos\theta_c)]$=finite and $\lim_{\alpha\to\infty}[\tilde{\psi}(\alpha,\theta_c)/\sqrt{\sinh\alpha}]$=finite. These two constraints for obtaining well-behaved liquid-phase transport require the evaporation rate to approach a constant value as α goes to infinity (the contact line). Therefore, the singular behavior of the gas-diffusion solution needs to be remedied to enable uniformly valid, physical solutions to be obtained for the liquid motion.

Fischer[15] assumed that the evaporative flux decays exponentially near the contact line ($\alpha>7$),

$$J(\alpha) = \begin{cases} J(\alpha), & \alpha\le 7 \\ J(7)\exp(7-\alpha), & \alpha>7. \end{cases} \tag{67}$$

We use the above when $\theta_c<90°$ and refer to the boundary condition for these cases as *modified diffusive evaporative flux*.

B. Cylindrical cap shape

As reported by Petsi and Burganos,[20]

$$\frac{d\theta_c}{dt} = -\frac{\sin^2\theta_c}{R\rho(1-\theta_c\cot\theta_c)}\int_0^\infty \frac{J(\alpha)}{\cosh\alpha+\cos\theta_c}d\alpha, \tag{68}$$

$$V_\theta(\alpha,\theta_c) = R(\cosh\alpha+\cos\theta_c)^{-1}(d\theta_c/dt) + J(\alpha)/\rho, \tag{69}$$

and

$$\psi(\alpha,\theta_c) = -\frac{d\theta_c}{dt}\frac{R^2}{\sin^2\theta_c}\left\{\frac{\sinh\alpha}{\cosh\alpha+\cos\theta_c} + \cot\theta_c \times\left[\sin^{-1}\left(\frac{1+\cosh\alpha\cos\theta_c}{\cosh\alpha+\cos\theta_c}\right) - \pi/2\right]\right\} - \frac{R}{\rho}\int_0^\alpha \frac{J(\alpha')}{\cosh\alpha'+\cos\theta_c}d\alpha'. \tag{70}$$

1. Uniform evaporative flux

In this case, the evaporative flux is uniform across the surface of the drop,

$$J(\alpha,\theta_c)=\text{const}=J_0. \tag{71}$$

Therefore,

$$\frac{d\theta_c}{dt}=-\frac{J_0}{R\rho}\frac{\theta_c\sin\theta_c}{1-\theta_c\cot\theta_c}, \tag{72}$$

$$V_\theta(\alpha,\theta_c)=(J_0/\rho)\{1-\theta_c\sin^2\theta_c/[(1-\theta_c\cot\theta_c)(\cosh\alpha+\cos\theta_c)]\}, \tag{73}$$

and

$$\psi(\alpha,\theta_c)=\frac{RJ_0}{\rho(\sin\theta_c-\theta_c\cos\theta_c)}\left[\frac{\theta_c\sinh\alpha}{\cosh\alpha+\cos\theta_c}+\sin^{-1}\left(\frac{1+\cosh\alpha\cos\theta_c}{\cosh\alpha+\cos\theta_c}\right)-\pi/2\right]. \tag{74}$$

Consequently,

$$\tilde{\tilde{\psi}}(\theta_c,\tau)=-\frac{RJ_0}{\rho(\tan\theta_c-\theta_c)}\left[\frac{\tan\theta_c\sinh\alpha}{\cosh\alpha+\cos\theta_c}+\sin^{-1}\left(\frac{1+\cosh\alpha\cos\theta_c}{\cosh\alpha+\cos\theta_c}\right)-\pi/2\right]. \tag{75}$$

2. Diffusive evaporative flux

Laplace's equation for gas diffusion outside a cylindrical cap drop does not allow an analytical solution when the outer boundary is at infinity since the solution varies logarithmically. Therefore, unlike the 3D axisymmetric case, a solution does not exist for diffusive evaporative flux in 2D.

IV. FREELY MOVING CONTACT LINE

When the droplet contact line is free to move (unpinned), the radial distance to the contact line decreases with time, $R=R(t)$. One condition previously considered in this case is that the contact angle remains constant during evaporation $\theta_c=\text{const}$.[10,20] This will also be assumed here. Since diffusive evaporative flux does not lead to an acceptable solution (see Secs. III A 2 and III B 2) only uniform flux will be considered as the boundary condition in what follows.

A. Spherical cap shape

As reported previously,[10]

$$\frac{dR}{dt}=-\frac{(1+\cos\theta_c)^2}{\sin\theta_c(1+\cos\theta_c/2)}\times\int_0^\infty\frac{\sinh\alpha}{(\cosh\alpha+\cos\theta_c)^2}\frac{J(\alpha)}{\rho}d\alpha, \tag{76}$$

$$V_\theta(\alpha,\theta_c)=\sin\theta_c\cosh\alpha(\cosh\alpha+\cos\theta_c)^{-1}(dR/dt)+J(\alpha)/\rho, \tag{77}$$

and

$$\psi(\alpha,\theta_c)=-\frac{dR}{dt}R^2\sin\theta_c\left[\frac{1+\cos\theta_c/2}{(1+\cos\theta_c)^2}-\frac{\cosh\alpha+\cos\theta_c/2}{(\cosh\alpha+\cos\theta_c)^2}\right]-\int_0^\alpha\frac{R^2\sinh\alpha'}{(\cosh\alpha'+\cos\theta_c)^2}\frac{J(\alpha')}{\rho}d\alpha'. \tag{78}$$

1. Uniform evaporative flux

In this case, the evaporative flux is uniform across the surface of the drop,

$$J(\alpha,\theta_c)=\text{const}=J_0. \tag{79}$$

Therefore,

$$\frac{dR}{dt}=-\frac{J_0}{\rho}\frac{1+\cos\theta_c}{\sin\theta_c(1+\cos\theta_c/2)}, \tag{80}$$

$$V_\theta(\alpha,\theta_c)=(J_0/\rho)\{1-[(1+\cos\theta_c)\cosh\alpha]/[(1+\cos\theta_c/2)(\cosh\alpha+\cos\theta_c)]\}, \tag{81}$$

and

$$\psi(\alpha,\theta_c)=-\frac{R^2J_0\cos\theta_c}{\rho(\cosh\alpha+\cos\theta_c)(2+\cos\theta_c)}\times\left(1-\frac{1+\cos\theta_c}{\cosh\alpha+\cos\theta_c}\right). \tag{82}$$

Consequently,

$$\tilde{\psi}(\theta_c,\tau)=\frac{R^2J_0\cos\theta_c}{\rho(2+\cos\theta_c)}\left[\sqrt{\cosh\alpha+\cos\theta_c}-\frac{\cos\theta_c/2}{\sqrt{\cosh\alpha+\cos\theta_c}}-\frac{4-(\cos\theta_c-3)^2/4}{(\cosh\alpha+\cos\theta_c)^{3/2}}+\frac{3\sin^2\theta_c(1+\cos\theta_c)/4}{(\cosh\alpha+\cos\theta_c)^{5/2}}\right]. \tag{83}$$

Using Eqs. (65) and (66),

$$K(\theta_c,\tau)=(R^2J_0/\rho)\cos\theta_c[\sqrt{2}(2+\cos\theta_c)\cosh\pi\tau]^{-1}\times[2\tau\cot(\theta_c/2)\sinh\theta_c\tau+\cosh\theta_c\tau] \tag{84}$$

and

$$\tilde{K}(\theta_c,\tau)=-\frac{R^2J_0\cos\theta_c/(2+\cos\theta_c)}{\rho\sqrt{8}\cosh\pi\tau\sin^2(\theta_c/2)}\times\{2\tau\sinh\theta_c\tau\cot(\theta_c/2)\times[\tau^2(\cos\theta_c-1)-2\cos\theta_c-1]+\cosh\theta_c\tau[\tau^2(5\cos\theta_c+7)-\cos\theta_c+1]\}. \tag{85}$$

B. Cylindrical cap shape

As reported by Petsi and Burganos,[20]

$$\frac{dR}{dt} = -\frac{\sin^2\theta_c}{\rho(\theta_c - \sin\theta_c\cos\theta_c)}\int_0^\infty \frac{J(\alpha)}{\cosh\alpha + \cos\theta_c}d\alpha, \tag{86}$$

$$V_\theta(\alpha,\theta_c) = \sin\theta_c\cosh\alpha(\cosh\alpha+\cos\theta_c)^{-1}(dR/dt) + J(\alpha)/\rho, \tag{87}$$

and

$$\psi(\alpha,\theta_c) = \frac{dR}{dt}\frac{R}{\sin^2\theta_c}\left[\frac{\sinh\alpha\sin\theta_c\cos\theta_c}{\cosh\alpha+\cos\theta_c} + \sin^{-1}\left(\frac{1+\cosh\alpha\cos\theta_c}{\cosh\alpha+\cos\theta_c}\right) - \pi/2\right] - \frac{R}{\rho}\int_0^\alpha \frac{J(\alpha')}{\cosh\alpha'+\cos\theta_c}d\alpha'. \tag{88}$$

1. Uniform evaporative flux

In this case, the evaporative flux is uniform across the surface of the drop,

$$J(\alpha,\theta_c) = \text{const} = J_0. \tag{89}$$

Therefore,

$$\frac{dR}{dt} = -\frac{J_0\,\theta_c\sin\theta_c}{\rho(\theta_c - \sin\theta_c\cos\theta_c)}, \tag{90}$$

$$V_\theta(\alpha,\theta_c) = (J_0/\rho)\{1 - \theta_c\sin^2\theta_c\cosh\alpha/[(\theta_c - \sin\theta_c\cos\theta_c)(\cosh\alpha+\cos\theta_c)]\}, \tag{91}$$

and

$$\psi(\alpha,\theta_c) = -\frac{J_0\cos\theta_c}{\rho(\theta_c-\sin\theta_c\cos\theta_c)}\times\left[\frac{\theta_c\sinh\alpha}{\cosh\alpha+\cos\theta_c} + \sin^{-1}\left(\frac{1+\cosh\alpha\cos\theta_c}{\cosh\alpha+\cos\theta_c}\right) - \pi/2\right]. \tag{92}$$

Consequently,

$$\tilde{\tilde{\psi}}(\theta_c,\tau) = \frac{RJ_0\cos^2\theta_c}{\rho(\theta_c-\sin\theta_c\cos\theta_c)}\left[\frac{\tan\theta_c\sinh\alpha}{\cosh\alpha+\cos\theta_c} + \sin^{-1}\left(\frac{1+\cosh\alpha\cos\theta_c}{\cosh\alpha+\cos\theta_c}\right) - \pi/2\right]. \tag{93}$$

V. RESULTS AND DISCUSSION

In this section, the velocity distributions for the present viscous flow analysis are compared to the previous distributions obtained for inviscid flow.[10] The cases of pinned and freely moving contact lines are computed for both the uniform evaporative flux and the modified diffusive evaporative flux boundary conditions. Flow patterns are illustrated for $\theta_c < 90°$ (wetting), $\theta_c = 90°$, and $\theta_c > 90°$ (nonwetting).

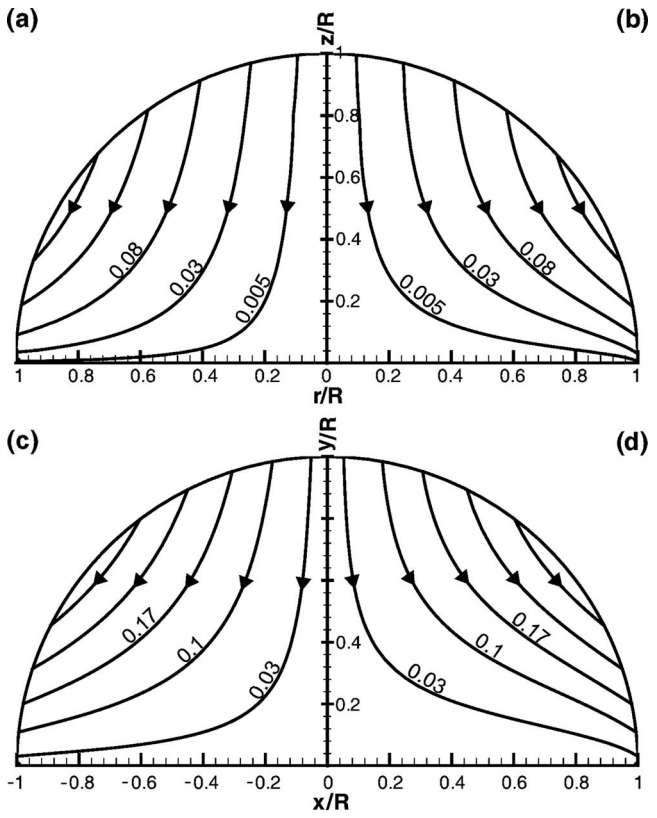

FIG. 3. Contours of nondimensional stream function for pinned contact lines with uniform=diffusive evaporative flux at $\theta_c = 90°$: (a) inviscid, spherical cap, (b) viscous, spherical cap ($\psi^*_{a,b}$=0.005, 0.03, 0.08, 0.15, and 0.22), (c) inviscid, cylindrical cap, and (d) viscous, cylindrical cap ($\psi^*_{c,d}$ =0.03, 0.01, 0.17, 0.24, and 0.3).

The results are presented in terms of the dimensionless stream function, $\psi^* = \psi/\psi_0$, and the dimensionless velocity, $V^* = V/V_0$. For axially symmetric flow,

$$\psi_0 = R^2 J_0/\rho, \tag{94}$$

and for planar flow,

$$\psi_0 = RJ_0/\rho. \tag{95}$$

For both flows,

$$V_0 = J_0/\rho. \tag{96}$$

where J_0 is the characteristic evaporative flux. For diffusive evaporation, J_0 is defined as

$$J_0 = \rho_g D(Y_s - Y_\infty)/R, \tag{97}$$

in which ρ_g is the density of the vapor-air mixture, D is the binary diffusion coefficient for vapor through air, Y_s is the mass fraction of vapor in the gas phase at the droplet surface (saturation), and Y_∞ is the mass fraction of vapor in the far field.

A. Viscous versus inviscid solutions

Figure 3 compares, for the pinned contact, the viscous and inviscid flows within hemispherical, Figs. 3(a) and 3(b), and hemicylindrical, Figs. 3(c) and 3(d), drops. For this case ($\theta_c = \pi/2$), the diffusive flux is uniform for both geometries. It is seen that in both cases, streamlines for viscous flow lie

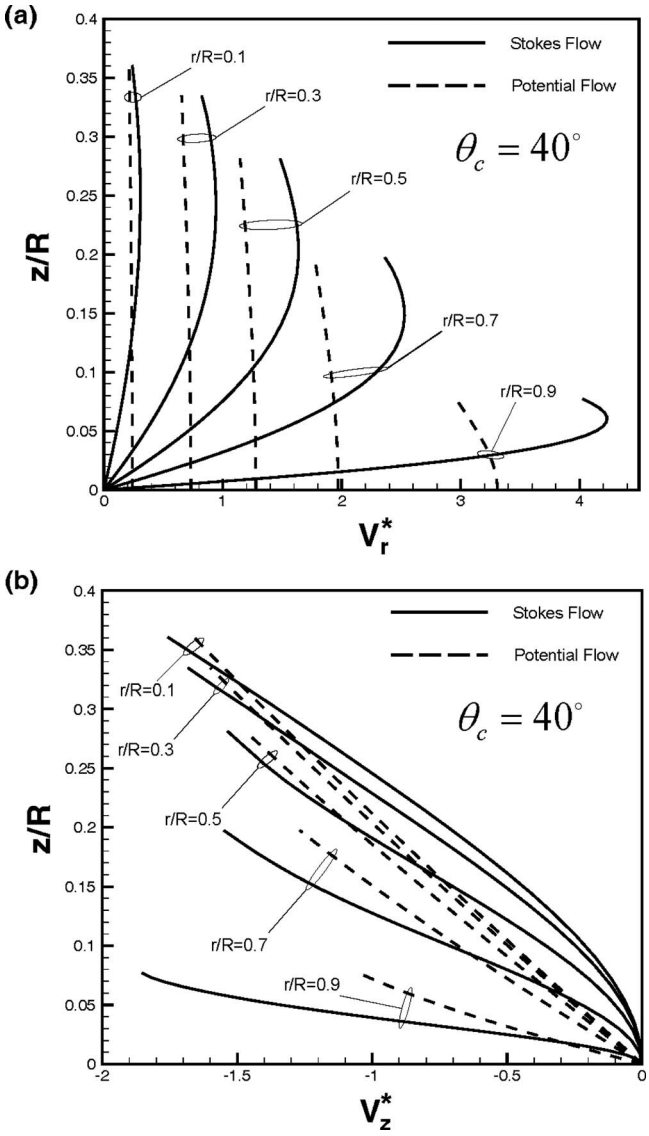

FIG. 4. Nondimensional velocities vs vertical position at different radial positions (r/R=0.1, 0.3, 0.5, 0.7, 0.9) for a pinned contact line, modified diffusive evaporative flux, and θ_c=40°. The dash lines are inviscid flow (Ref. 10); the solid lines are viscous flow. (a) Radial velocity; (b) vertical velocity.

farther from the substrate than the corresponding streamlines for inviscid flow. On the other hand, since both viscous and inviscid flows follow the same boundary conditions at the free surface, the flows behave similarly near the droplet surface.

For the modified diffusive evaporative flux, Fig. 4 compares the vertical and radial velocities for inviscid flow to those in viscous flow for pinned contacts with θ_c=40°. As r/R increases, significant differences are observed in the radial velocities due to the no slip condition at the solid surface. The vertical velocities are qualitatively the same although they differ in magnitude.

In Fig. 4 the contact angle is set to 40° so that the present results could be compared directly with the numerical solution by Hu and Larson.[16] Their solution was only presented graphically. Laying Fig. 4 of this study over Fig. 5 of Ref. 16 showed that the lines were congruent.

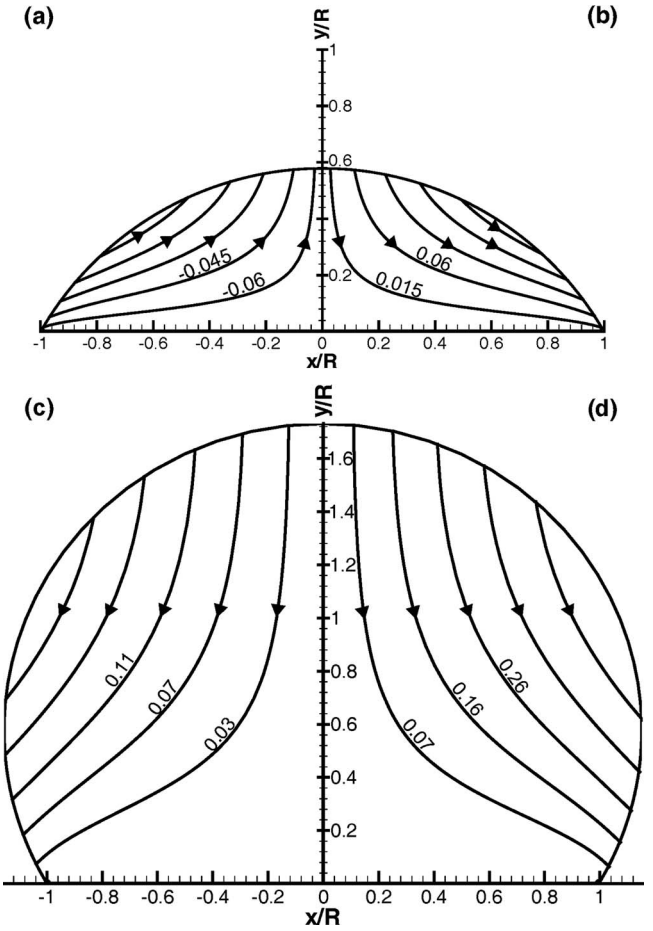

FIG. 5. Contours of nondimensional stream function for viscous flow inside a cylindrical cap exposed to uniform flux (a) θ_c=60°, freely moving contact line (ψ^*=−0.06, −0.045, −0.03, −0.015, and −0.004), (b) θ_c=60°, pinned contact line (ψ^*=0.015, 0.06, 0.115, 0.17, and 0.22), (c) θ_c=120°, freely moving contact line (ψ^*=0.03, 0.07, 0.11, 0.15, and 0.185), and (d) θ_c=120°, pinned contact line (ψ^*=0.07, 0.16, 0.26, 0.36, and 0.46).

B. Uniform flux

Since spherical and cylindrical cap drops exhibit the same behavior for various evaporative fluxes, the results for cylindrical cap drops will be used to illustrate the flow structures corresponding to a uniform evaporative flux. The flow patterns computed for different contact angles and contact line conditions are illustrated in Fig. 5. It can be seen that when the contact line is pinned, the flow is from the center of the drop to its edge. On the other hand, when the contact line is free to move, distinctively different flow patterns are observed for wetting ($\theta_c < \pi/2$) and nonwetting ($\theta_c > \pi/2$) conditions—see Figs. 5(a) and 5(c). (This is consistent with the behavior in inviscid flow.[10,19])

C. Modified diffusive evaporative flux

It is shown in Ref. 9 that (i) for $\theta_c > 90°$, the evaporative flux decays to zero as $(r/R) \to 1$, (ii) for θ_c=90°, the evaporation rate is uniform over the free surface, and (iii) for $\theta_c < 90°$, the evaporation rate diverges at the contact line. In

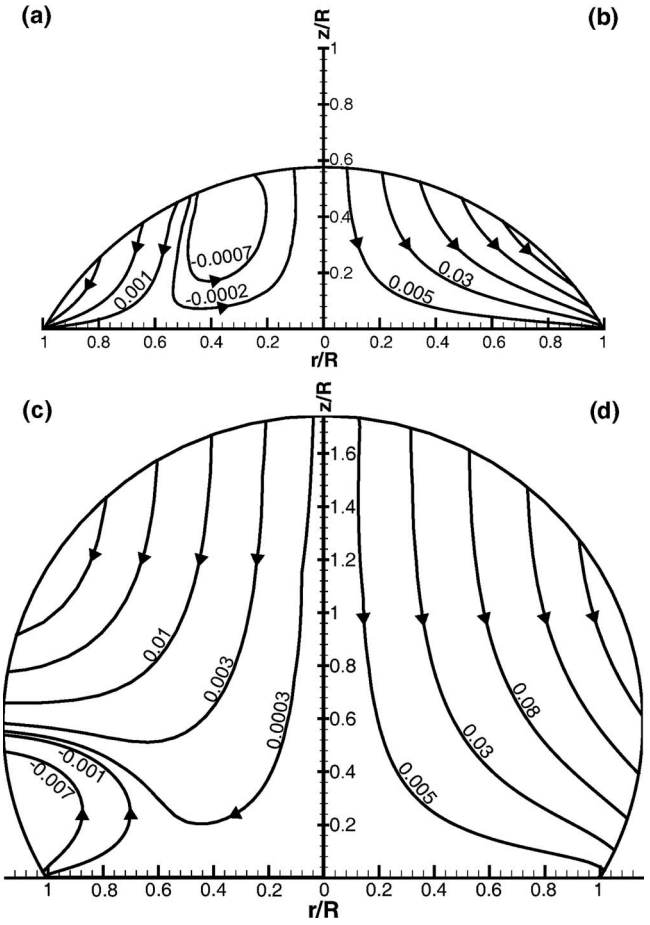

FIG. 6. Contours of nondimensional stream function for viscous flow inside a spherical cap exposed to modified diffusive evaporative flux (a) $\theta_c=60°$, freely moving contact line ($\psi^*=-0.0007$, -0.0002, 0.001, 0.006, and 0.02), (b) $\theta_c=60°$, pinned contact line ($\psi^*=0.005$, 0.03, 0.08, 0.15, and 0.22), (c) $\theta_c=120°$, freely moving contact line ($\psi^*=-0.007$, -0.001, 0.0003, 0.003, 0.01, 0.02, and 0.03), and (d) $\theta_c=120°$, pinned contact line ($\psi^*=0.005$, 0.03, 0.08, 0.15, and 0.22).

order to prevent the nonphysical divergence when $\theta_c<90°$, modified diffusive evaporative flux has been used as the boundary condition.

Figure 6 presents the four cases considered: $\theta_c=60°$ and 120° for both pinned and freely moving contact lines. When the contact line is pinned, the flow is directed from the center of the drop to its edges ("coffee-ring" phenomenon). The flow behavior remains the same even for contact angles greater than 90° where the evaporative flux distribution is quite different. On the other hand, when the contact line is freely moving, the flow pattern is more intricate. In a given drop, fluid flows both toward and away from the edge, making it unlikely that a colloidal drop would deposit a coffee-ring pattern of particles.

ACKNOWLEDGMENTS

The importance of this problem was brought to our attention by Professor R. C. Wetherhold.

APPENDIX A: $E^4\psi=0$, TOROIDAL COORDINATES—SEPARATION OF VARIABLES SOLUTION

Similar to Khuri and Waswaz,[23] an "R-separable" form is assumed to separate variables for $E^4\psi=0$ in toroidal coordinates. The form assumed here is

$$\psi(\alpha,\theta)=(\cosh\alpha+\cos\theta)^{-3/2}\phi(\alpha,\theta). \tag{A1}$$

(Khuri and Waswaz[23] assumed $R\sinh\alpha$ times the above.) Substituting Eq. (A1) into Eq. (9) and then repeating the E^2 operation leads to

$$\frac{\partial^4\phi}{\partial\alpha^4}+2\frac{\partial^4\phi}{\partial\alpha^2\,\partial\theta^2}+\frac{\partial^4\phi}{\partial\theta^4}-2\coth\alpha\frac{\partial^3\phi}{\partial\alpha^3}-2\coth\alpha\frac{\partial^3\phi}{\partial\alpha\,\partial\theta^2}+(3\coth^2\alpha-3.5)\frac{\partial^2\phi}{\partial\alpha^2}+(5/4)\frac{\partial^2\phi}{\partial\theta^2}+\coth\alpha(4.5-3\coth^2\alpha)\frac{\partial\phi}{\partial\alpha}+(9/16)\phi=0. \tag{A2}$$

Assuming a product form for separating variables in Eq. (A2),

$$\phi(\alpha,\theta)=f(\alpha)g(\theta), \tag{A3}$$

leads to

$$g^{(4)}+2\left[\frac{f^{(2)}}{f}-\coth\alpha\frac{f^{(1)}}{f}+5/4\right]g^{(2)}+\left[\frac{f^{(4)}}{f}-2\coth\alpha\frac{f^{(3)}}{f}+(3\coth^2\alpha-3.5)\frac{f^{(2)}}{f}+\coth\alpha(4.5-3\coth^2\alpha)\frac{f^{(1)}}{f}+9/16\right]g=0. \tag{A4}$$

To be consistent with the assumed separable form, Eq. (A3), the two bracketed coefficients in Eq. (A4) must be constants. Denoting the constant for the first bracket as $(1-\tau^2)$ (in order to obtain an established differential equation for the eigenfunctions in α), the Gegenbauer equation is obtained

$$f^{(2)}-\coth\alpha f^{(1)}+(\tau^2+1/4)f=0. \tag{A5}$$

The solution to Eq. (A5) is

$$f(\alpha)=A(\tau)C^{-1/2}_{1/2+i\tau}(\cosh\alpha)+B(\tau)C^{*-1/2}_{1/2+i\tau}(\cosh\alpha).$$

Using Eq. (A5) and its first and second derivatives, the second bracketed coefficient in Eq. (A4) is readily shown to be

$$\frac{f^{(4)}}{f}-2\coth\alpha\frac{f^{(3)}}{f}+(3\coth^2\alpha-3.5)\frac{f^{(2)}}{f}+\coth\alpha(4.5-3\coth^2\alpha)\frac{f^{(1)}}{f}+9/16=(\tau^2+1)^2. \tag{A6}$$

Inserting the above constant values for the first and second brackets, Eq. (A4) becomes

$$\frac{d^4g}{d\theta^4} + 2(1-\tau^2)\frac{d^2g}{d\theta^2} + (\tau^2+1)^2 g = 0. \tag{A7}$$

The solution to this constant coefficient equation follows directly and is given by

$$g(\theta) = \sinh(\tau\theta)[C(\tau)\sin\theta + D(\tau)\cos\theta] + \cosh(\tau\theta)[E(\tau)\sin\theta + F(\tau)\cos\theta], \tag{A8}$$

where, $C(\tau)$, $D(\tau)$, $E(\tau)$, and $F(\tau)$ are real functions. Since $0 \le \alpha < \infty$, the associated eigenvalues are continuously distributed: $0 \le \tau < \infty$. The general solution is then

$$\psi(\alpha,\theta) = (\cosh\alpha + \cos\theta)^{-3/2}\int_0^\infty [A(\tau)C^{-1/2}_{1/2+i\tau}(\cosh\alpha) + B(\tau)C^{*-1/2}_{1/2+i\tau}(\cosh\alpha)] \times \{\sinh(\tau\theta)[C(\tau)\sin\theta + D(\tau)\cos\theta] + \cosh(\tau\theta)[E(\tau)\sin\theta + F(\tau)\cos\theta]\}d\tau. \tag{A9}$$

APPENDIX B: $\nabla^4\psi = 0$, BIPOLAR COORDINATES—SEPARATION OF VARIABLES SOLUTION

Following the analysis of Jeffery,[25] the biharmonic equation $\nabla^4\psi = 0$) may be R-separated in bipolar coordinates by assuming

$$\psi(\alpha,\theta) = (\cosh\alpha + \cos\theta)^{-1}\phi(\alpha,\theta). \tag{B1}$$

Substituting Eq. (B1) into Eq. (45) and then repeating the ∇^2 operation leads to

$$\frac{\partial^4\phi}{\partial\alpha^4} + 2\frac{\partial^4\phi}{\partial\alpha^2\,\partial\theta^2} + \frac{\partial^4\phi}{\partial\theta^4} - 2\frac{\partial^2\phi}{\partial\alpha^2} + 2\frac{\partial^2\phi}{\partial\theta^2} + \phi = 0. \tag{B2}$$

Assuming the variables are separable, $\phi(\alpha,\theta) = f(\alpha)g(\theta)$, Eq. (B2) becomes

$$g^{(4)} + 2\left(\frac{f^{(2)}}{f} + 1\right)g^{(2)} + \left(\frac{f^{(4)}}{f} - 2\frac{f^{(2)}}{f} + 1\right)g = 0. \tag{B3}$$

Since g was assumed to be independent of α, the coefficients of $g^{(2)}$ and g must be constants. Setting the coefficient of $g^{(2)}$ equal to $2(1-\tau^2)$,

$$f^{(2)}/f = -\tau^2, \tag{B4}$$

where the form of the constant was chosen to obtain eigenfunctions in α. The solution of Eq. (B4) is

$$f(\alpha) = A(\tau)\sin(\tau\alpha) + B(\tau)\cos(\tau\alpha). \tag{B5}$$

Substituting this into the coefficient of g yields

$$\frac{f^{(4)}}{f} - 2\frac{f^{(2)}}{f} + 1 = (\tau^2+1)^2. \tag{B6}$$

Consequently, the differential equation for $g(\theta)$ is

$$\frac{d^4g}{d\theta^4} + 2(1-\tau^2)\frac{d^2g}{d\theta^2} + (\tau^2+1)^2 g = 0. \tag{B7}$$

Note that this equation in bipolar coordinates is identical to the corresponding equation in toroidal coordinates, Eq. (A7). The solution for the stream function is therefore

$$\psi(\alpha,\theta) = (\cosh\alpha + \cos\theta)^{-1}\int_0^\infty [A(\tau)\sin(\tau\alpha) + B(\tau)\cos(\tau\alpha)] \times \sinh(\tau\theta)[C(\tau)\sin\theta + D(\tau)\cos\theta] + \cosh(\tau\theta)[E(\tau)\sin\theta + F(\tau)\cos\theta]d\tau. \tag{B8}$$

[1] S. Maenosono, C. D. Dushkin, S. Saita, and Y. Yamaguchi, "Growth of a semiconductor nanoparticle ring during the drying of a suspension droplet," Langmuir **15**, 957 (1999).
[2] M. Chopra, L. Li, H. Hu, M. A. Burns, and R. G. Larson, "DNA molecular configurations in an evaporating droplet near a glass surface," J. Rheol. **47**, 1111 (2003).
[3] N. D. Denkov, O. D. Velev, P. A. Kralchevsky, I. B. Ivanov, H. Yoshimura, and K. Nagayama, "Mechanism of formation of 2-dimensional crystals from latex-particles on substrates," Langmuir **8**, 3183 (1992).
[4] A. S. Dimitrov, C. D. Dushkin, H. Yoshimura, and K. Nagayama, "Mechanism of formation of 2-dimensional crystals from latex-particles on substrates," Langmuir **10**, 432 (1994).
[5] C. D. Dushkin, H. Yoshimura, and K. Nagayama, "Nucleation and growth of 2-dimensional colloidal crystals," Chem. Phys. Lett. **204**, 455 (1993).
[6] R. G. Larson, T. T. Perkins, D. E. Smith, and S. Chu, "Hydrodynamics of a DNA molecule in a flow field," Phys. Rev. E **55**, 1794 (1997).
[7] N. R. Bieri, J. Chung, S. E. Haferl, D. Poulikakos, and C. P. Grigoropoulos, "Microstructuring by printing and laser curing of nanoparticle solutions," Appl. Phys. Lett. **82**, 3529 (2003).
[8] H. Sirringhaus, T. Kawase, R. H. Friend, T. Shimoda, M. Inbasekaran, W. Wu, and E. P. Woo, "High-resolution inkjet printing of all-polymer transistor circuits," Science **290**, 2123 (2000).
[9] J. B. Szczech, C. M. Megaridis, J. Zhang, and D. R. Gamota, "Ink jet processing of metallic nanoparticle suspensions for electronic circuitry fabrication," Microscale Thermophys. Eng. **8**, 327 (2004).
[10] H. Masoud and J. D. Felske, "Analytical solution for inviscid flow inside an evaporating sessile drop," Phys. Rev. E **79**, 016301 (2009).
[11] R. D. Deegan, "Pattern formation in drying drops," Phys. Rev. E **61**, 475 (2000).
[12] R. D. Deegan, O. Bakajin, T. F. Dupont, G. Huber, S. R. Nagel, and T. A. Witten, "Capillary flow as the cause of ring stains from dried liquid drops," Nature (London) **389**, 827 (1997).
[13] R. D. Deegan, O. Bakajin, T. F. Dupont, G. Huber, S. R. Nagel, and T. A. Witten, "Contact line deposits in an evaporating drop," Phys. Rev. E **62**, 756 (2000).
[14] Y. O. Popov, "Evaporative deposition patterns: Spatial dimensions of the deposit," Phys. Rev. E **71**, 036313 (2005).
[15] B. J. Fischer, "Particle convection in an evaporating colloidal droplet," Langmuir **18**, 60 (2002).
[16] H. Hu and R. G. Larson, "Analysis of the microfluid flow in an evaporating sessile droplet," Langmuir **21**, 3963 (2005).
[17] E. Widjaja and M. T. Harris, "Numerical study of vapor phase-diffusion driven sessile drop evaporation," Comput. Chem. Eng. **32**, 2169 (2008).
[18] Y. Y. Tarasevich, "Simple analytical model of capillary flow in an evaporating sessile drop," Phys. Rev. E **71**, 027301 (2005).
[19] A. J. Petsi and V. N. Burganos, "Potential flow inside an evaporating cylindrical line," Phys. Rev. E **72**, 047301 (2005).
[20] A. J. Petsi and V. N. Burganos, "Evaporation-induced flow in an inviscid liquid line at any contact angle," Phys. Rev. E **73**, 041201 (2006).
[21] M. Stimson and G. B. Jeffery, "The motion of two spheres in a viscous fluid," Proc. R. Soc. London, Ser. A **111**, 110 (1926).
[22] L. E. Payne and W. H. Pell, "The Stokes flow problem for a class of axially symmetric bodies: The Stokes flow problem for a class of axially symmetric bodies," J. Fluid Mech. **7**, 529 (1960).
[23] S. A. Khuri and A. M. Wazwaz, "On the solution of a partial differential equation arising in Stokes flow," Appl. Math. Comput. **85**, 139 (1997).
[24] J. Happel and H. Brenner, in *Low Reynolds Number Hydrodynamics: With Special Applications to Particulate Media*, 1st ed., edited by M. Nijhoff (Kluwer, Boston, 1983).
[25] G. B. Jeffery, "On a form of the solution of Laplace's equation suitable for problems relating to two spheres," Philos. Trans. R. Soc. London, Ser. A **221**, 265 (1921).